Reports

X-Ray Diffraction Evidence for Nonstoichiometric Rubidium-C_{60} Intercalation Compounds

QING ZHU, OTTO ZHOU, NICOLE COUSTEL, GAVIN B. M. VAUGHAN, JOHN P. MCCAULEY, JR., WILLIAM J. ROMANOW, JOHN E. FISCHER,* AMOS B. SMITH III

Powder x-ray diffraction at 300 K on equilibrated samples of several nominal compositions x in Rb_xC_{60} is reported. In addition to the face-centered cubic (fcc) (x = 3, superconducting), body-centered tetragonal (x = 4), and body-centered cubic (bcc) (x = 6) stoichiometric phases, direct evidence for a dilute fcc doped phase, $0 < x \leq 1$, and for a substoichiometric bcc phase, $x \sim 5$, is presented. In contrast, x = 3 and x = 4 appear to be line phases with nearly zero solubility of Rb vacancies and interstitials at 300 K. These results are summarized in a provisional binary phase diagram.

ALKALI METAL–INTERCALATED C_{60} is now established as an important new family of synthetic metals. Four distinct phases have been identified in the binary system M_xC_{60} with M = K or Rb, namely face-centered cubic (fcc)(I) at $x = 0$ (*1, 2*), the superconducting phase fcc(II) for which $x = 3$ (*3–6*), a body-centered tetragonal (bct) phase at $x = 4$ (*7*), and the saturated body-centered cubic phase (bcc) of ideal stoichiometry, $x = 6$ (*8*). We present x-ray evidence that fcc(I) and bcc are stable phases over finite ranges of x at 300 K, while fcc(II) and bct appear to be line compounds (that is, only one value of x). The resulting provisional phase diagram has some features in common with those of the better known layer intercalates (*9*) and doped conjugated polymers (*10*).

Since the initial discovery of the bcc ordered superlattice, it has become clear that great care must be taken to ensure equilibrium in the synthesis of these materials when $x < 6$. The bcc K, Rb, and Cs compounds are reproducibly obtained under rather mild vapor phase conditions (typically 225°C for 24 hours), but much longer times (*6*) or higher temperatures (T) (*4, 5*), or both, are necessary to obtain reasonably pure phases of fcc(II) and bct. Accumulated experience on the synthesis of bulk powder samples suggests the importance of reexamining some of the conclusions or inferences concerning phase equilibria based upon in situ doped film measurements (*11, 12*), which necessarily involve milder synthesis conditions than the powder preparations.

We also considered the M_xC_{60} system in the more general context of guest-host intercalation systems, analogous to intercalated layer compounds and doped conjugated polymers. In general, strongly anisotropic host lattices are responsible for competing attractive and repulsive guest-guest interactions, which in turn are the origin of concentration-dependent superlattice structures ("stages") at low temperature (*9, 10, 13*). A qualitatively different competition might be envisaged in M_xC_{60} between electrostatic and elastic effects that would enhance the stability of high- and low-concentration phases, respectively. Regardless of the energetic details, entropy dominates at sufficiently high T for any guest-host system, and the guest distribution is then expected to be completely random for all concentrations. The first-order phase boundaries between low-T superlattices and the high-T lattice gas or liquid phase imply finite formation energies for vacancies and interstitials (such as nonstoichiometric phases) near the $x = 0$ and $x = 6$ extremities of the phase diagram. The present work was motivated in part by a search for such phases.

Powder samples of a desired global x were prepared by reacting appropriate relative amounts of C_{60} and saturation-doped M_6C_{60} as described previously (*5*). This differs from the more typical procedure of reacting preweighed M and C_{60} (*3, 4, 6, 7*). The final step typically consisted of annealing at 400° to 450°C for 1 hour to several days. Samples were then sealed in quartz capillaries in an argon atmosphere. Similar results were obtained for Rb_xC_{60} and K_xC_{60}. Most of the measurements were performed at the National Synchrotron Light Source X10A beamline.

Diffraction patterns were obtained for samples with global x values of 2.9, 3.3, and 4 (Fig. 1). The first two are dominated by the fcc(II) phase but contain small amounts of different minority phases (Fig. 2). All of the reflections in the $x = 2.9$ sample exhibit high-Q (where $Q = 4\pi\sin\theta/\lambda$) shoulders, the positions and approximate intensities of which can be determined by composite two-peak fits (Fig. 2, top). This indicates the presence of two fcc phases with slightly different lattice constants. In contrast, the $x = 3.3$ sample exhibits weak but resolved peaks from a different Bravais lattice (Fig. 2, bottom). The majority phase in both samples gives the same fcc lattice constant, a = 14.42 ± 0.02 Å, and the same relative integrated intensities (Fig. 3A). Both samples showed 55 to 60% diamagnetic shielding at 4 K and superconducting transition temperature T_c = 29.7 K, consistent with comparable amounts of a single superconducting phase in the two samples. We identify this phase as fcc(II) and conclude that this is a line compound at 300 K. Small deviations from stoichiometry lead to phase separation up to some T_{max}, above which the miscibility gap is permitted to vanish by symmetry as in layer intercalates (*9*).

Composite fits of the high-Q shoulders from the $x = 2.9$ profile give an average fcc lattice constant of 14.28 ± 0.09 Å. The large uncertainty is due to the weak shoulder intensities and to ambiguities in the lineshape model; the best fits (as presented in Fig. 2) were obtained with pure Gaussians

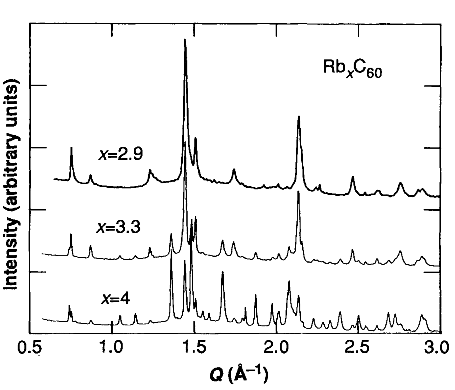

Fig. 1. X-ray powder diffractograms for $Rb_{2.9}C_{60}$ (top curve), $Rb_{3.3}C_{60}$ (middle curve), and Rb_4C_{60} (bottom curve). These profiles were measured on the NSLS X10A beamline with λ = 1.5289 Å.

Q. Zhu, O. Zhou, N. Coustel, J. E. Fisher, Materials Science and Engineering Department and Laboratory for Research on the Structure of Matter, University of Pennsylvania, Philadelphia, PA 19104.
G. B. M. Vaughan, Physics Department and Laboratory for Research on the Structure of Matter, University of Pennsylvania, Philadelphia, PA 19104.
J. P. McCauley, Jr., and A. B. Smith III, Chemistry Department and Laboratory for Research on the Structure of Matter, University of Pennsylvania, Philadelphia, PA 19104.
W. J. Romanow, Laboratory for Research on the Structure of Matter, University of Pennsylvania, Philadelphia, PA 19104.

---

*To whom correspondence should be sent.

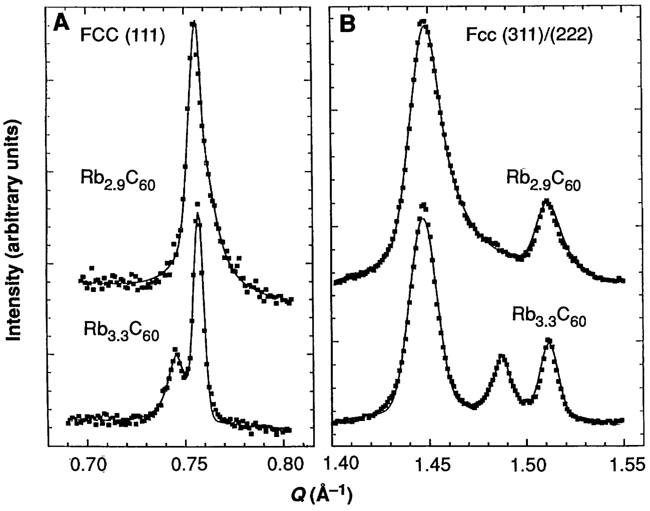

Fig. 2. Expanded view of the (**A**) fcc 111 and (**B**) fcc 311 and 222 reflections for $Rb_{2.9}C_{60}$ (top) and $Rb_{3.3}C_{60}$ (bottom). Solid curves are fits to the data. For $x = 2.9$, each peak is fit with two closely spaced lines representing coexisting fcc phases with slightly different a values. For $x = 3.3$, resolved peaks from a second, bct phase are found.

and Lorentzians for the majority and minority phase fcc reflections, respectively. Within this uncertainty, the minority phase **a** is marginally greater than the 14.18 Å value for fcc(I) at $x = 0$, but significantly smaller than the fcc(II) value. Convincing evidence that the shoulders signify a dilute doped phase rather than unreacted C_{60} is provided by the relative intensities, which are completely inconsistent with $x = 0$ (Fig. 3B). The fitted integrated intensities of the minority phase 111 and 220 reflections are much weaker than those of the 311, independent of the choice of lineshape used to model the two phases. This is in contrast to pure C_{60}, for which these reflections all have comparable intensities (*2*). Furthermore, the 200 reflection at 0.88 $Å^{-1}$ is also a composite two-component peak (not visible on the scale of Fig. 1); the presence of finite 200 intensity is further proof that the minority fcc phase is not undoped C_{60} (*2*).

We conclude that the minority constituent in the $x = 2.9$ sample is a dilute fcc(I) doped phase, the composition of which can be determined in principle either from the lever rule and the individual total scattered intensities of the fcc(I) and fcc(II) constituents, or by comparing the fcc(I) relative intensities with model calculations. The former approach is ruled out by even a small uncertainty in global x; an error of 0.05 translates into a 100% error in minority phase Rb concentration. The second suffers from the large uncertainties in fitted intensities; our best estimate is $x \leq 1$.

We ascribe the minority phase in the $x = 3.3$ profile to bct Rb_4C_{60} (*7*). The bottom profile in Fig. 1 ($x \sim 4$) is dominated by bct reflections with a smaller fcc(II) constituent. The bct reflections in both samples give the same lattice parameters as a pure-phase sample (**a** = 11.96 Å and **c** = 10.98 Å), from which we conclude that bct is also a line compound at 300 K. The miscibility gap between fcc(II) and bct will extend all the way to the melting point because of the different symmetries, but the range of unstable compositions is very likely to be T-dependent for entropic reasons. We found no diamagnetic shielding in a pure-phase sample of Rb_4C_{60} down to 5 K, in agreement with (*7*).

X-ray profiles were obtained for a sample with nominal Rb concentration $x = 5$, and a saturation-doped sample of nominal $x = 6$ (Fig. 4, top and bottom). Both are dominated by reflections that index as bcc, and the saturation-doped sample shows no evidence of a minority phase. The $x = 5$ sample contains only a small amount of bct, implying that the bcc component has an x value substantially less than 6. The inset to Fig. 4 shows directly that the bcc lattice constant in the $x = 5$ sample must be significantly smaller than in the $x = 6$ sample; the values are 11.47 ± 0.02 Å and 11.54 ± 0.01 Å, respectively. The identification of substoichiometric bcc is confirmed by analysis of the integrated intensities, which are particularly sensitive to M site occupation at low angles. Observed values for the 110 (0.78 $Å^{-1}$) and 211 (1.35 $Å^{-1}$) reflections are 5.0 and 3.4, respectively (strongest peak = 100), while those calculated for 83% (100%) occupancy of distorted tetrahedral sites are 5.6 (14.2) and 3.4 (0.2). The observation of a single bcc phase in nominal Rb_5C_{60} demonstrates that bcc is not a line compound. The bct → bcc transition must be first order by symmetry, therefore the miscibility gap must extend up to the melting point.

We summarize these results in a schematic phase diagram (Fig. 5) depicting the coexistence features of T- and x-dependent structures. The temperature scale is defined approximately by the 300 K label (lower left). The composition axis is dominated at low T by regions of two-phase coexistence. The first such region, $0 < x < 3$, is analogous to Safran's model for layer intercalates (*9*) since the end points are isostructural, that is, the (one-dimensional) superlattice symmetry is independent of x. On the other hand, we find no evidence for staging in this region, as would be expected from, for example, selective occupancy of octahedral sites at $x = 1$ (*14*). Further work is necessary to determine if the structure exemplified by the minority fcc(I) constituent (Figs. 1 to 3) is such an ordered stoichiometric phase. ^{13}C nuclear magnetic resonance shows phase separation in samples with global $x = 1.5$ and 2.0 (*15*), consistent with the present results. A better analogy for the second two coexistence regions, $3 < x < 4$ and $4 < x < 6$ at $T = 0$, is the potassium-polyacetylene–doped polymer system, in which the two-dimensional superlattice symmetry changes discontinuously with chemical potential (*16*). Additional evidence that fcc(II) is a stoichiometric compound is the observation that the superconducting T_c in different samples from different laboratories varies only from 29.6 K to 30 K.

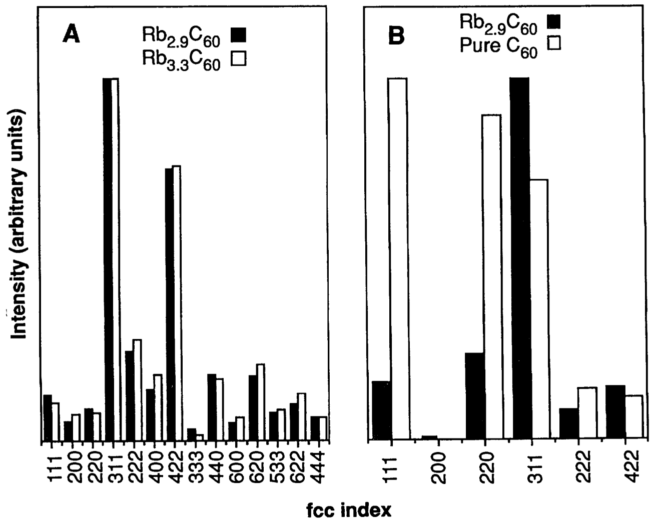

Fig. 3. Integrated intensities of the various fcc phases observed in the two samples of Figs. 1 and 2. (**A**) Majority phase intensities, showing that the same phase is present in both samples; (**B**) minority phase shoulders in the $x = 2.9$ sample, compared with the intensities of undoped C_{60}.

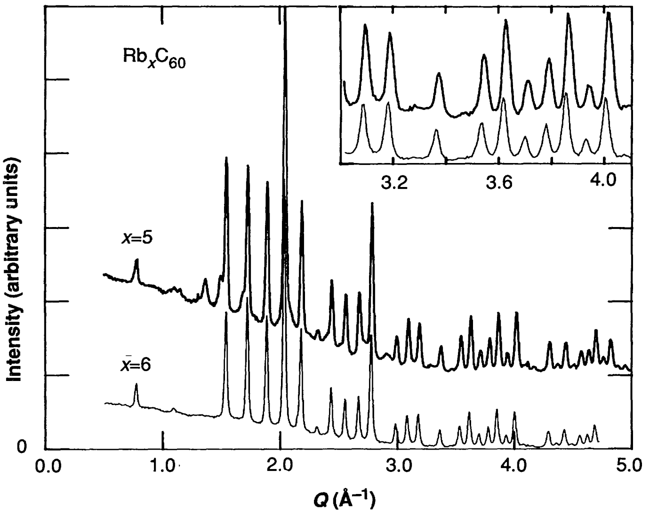

Fig. 4. Diffractograms for Rb_5C_{60} (top curve) and Rb_6C_{60} (bottom curve). The inset shows that the majority bcc phase has a different lattice constant in the two samples. These were measured on a standard diffractometer equipped with a sealed Cu tube.

A recent calculation shows that at $x = 3$, the Fermi energy is located in the conduction band such that the density of states, hence T_c, would be strongly enhanced by a small vacancy concentration (*17*).

The asymmetric upper boundary for $0 < x < 3$ separates mixed-phase fcc(I) + fcc(II) from the uniform high-T lattice gas or liquid (*9, 10, 13*) (Fig. 5). The asymmetry is a consequence of a nonvanishing and T-dependent density of random interstitials in fcc(I) and approximately zero vacancy density in fcc(II). The details of the steeper boundaries delineating fcc(II) + bct and bct + bcc will depend on the interplay between vacancy formation energies, configurational entropy of filled and empty sites, and elastic strains induced by x-driven symmetry transformations. The asymmetry for $4 < x < 6$ is reminiscent of a model for graphite intercalation compounds which takes into account elastic dilation of the host lattice (*18*); the smaller the concentration, the lower the strain, hence the more stable the phase mixture against an entropy-driven order-disorder transition. Corresponding strain in M_xC_{60} could be associated with shear distortions from fcc(II) to bct and from bct to bcc. In this context it is interesting to note that the volume per C_{60} molecule is anomalously large in the bct phase, despite the monotonic increase in M concentration. Using the above lattice constants, we find that the excess volume per molecule relative to fcc(I) ($x = 0$) is 41, 84, 50, and 65 Å^3 at $x = 3$, 4, 5, and 6, respectively.

Thus far, all the structural analyses of M_xC_{60} have assumed perfect crystallinity. To check this, we examined the Q dependence of the fitted Gaussian widths from the $x = 2.9$ phase (Fig. 6). The overall behavior, ΔQ increasing roughly linearly with Q, is consistent with a combination of instrumental resolution and sample strain. Superposed on this trend are pronounced minima at the 111, 222, 333, and 444 positions, suggesting that reflections with $h \neq k \neq l$ are anomalously broad owing to stacking faults between close-packed (111) planes. This idea is supported by the weaker but monotonic increase of ΔQ with increasing Q observed in all of our M_6C_{60} (bcc) samples, which do not contain close-packed molecular layers. Similar faulting has been identified by electron diffraction in the undoped fcc(I) structure (*19*), in which the fault density can be minimized by extended annealing. It is unclear at this point whether stacking faults are intrinsic to the fcc(II) structure, are controlled by the growth process, or are generated and stabilized by the presence of the minority fcc(I) component, or a combination of all three. The effect is so strong in our $x = 2.9$ profile that a reliable Rietfeld refinement could not be obtained, necessitating the integrated intensity analysis described above.

We also performed a Rietfeld refinement on a high-resolution profile of Rb_6C_{60}. The results are consistent with our previous work on K_6C_{60} and Cs_6C_{60} (*8*). The details for all three bcc phases will be presented elsewhere. Briefly, we obtain an integrated intensity R factor of 4.5% in space group Im3 (a = 11.536 Å), assuming a single but variable C-C intramolecular bond length. The molecules are oriented with twofold axes along cube edges. Carbon atom positions are localized to within a mean thermal displacement of 0.15 Å, and the best fit molecular radius is 3.57 Å (C-C bond length 1.44 Å), slightly dilated with respect to the 3.52 Å value obtained in fcc(I) and consistent with ab initio molecular dynamics simulations (*20*). Rb ions are relaxed from their ideal tetrahedral positions to (0, 0.28, 0.5) and symmetry-derived positions, also consistent with molecular dynamics. The center-to-center intermolecular distance is 9.98 Å, intermediate between the values for K_6C_{60} and Cs_6C_{60} and very close to the fcc(I) value.

A novel feature of the alkali metal-C_{60} system is the x dependence of T_{mo}, the molecular orientational ordering transition temperature. This transition has no counterpart in layer intercalates or doped polymers. What is known so far is that $T_{mo}(0) = 249$ K (*2*) and $T_{mo}(6) > 300$ K (*8*). In fcc(II) at 300 K, the C_{60}'s are variously claimed to be partitioned between two discrete orientations (*3*) or freely rotating (*15*). A particularly intriguing case is bct, in which the molecular point group symmetry is incompatible with the long-range order of the Bravais lattice (*7*). Further detailed studies of phase equilibria in M_xC_{60} intercalation compounds will be important for understanding and controlling the properties of synthetic metals and superconductors based on these solids.

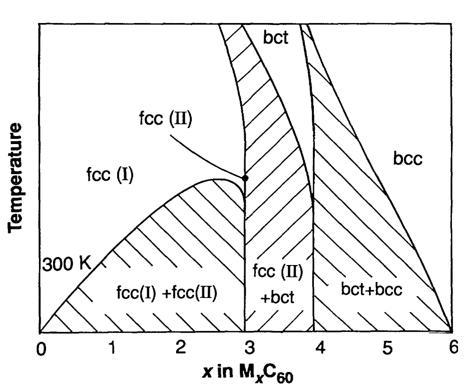

Fig. 5. Provisional, and very schematic, phase diagram for the alkali metal–solid C_{60} system. Shaded regions denote two-phase coexistence. The (linear) temperature scale is approximately indicated by the 300 K label in the lower left corner.

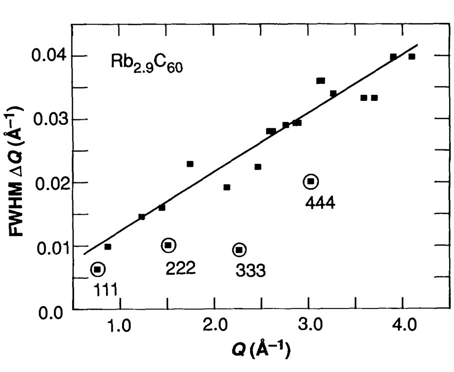

Fig. 6. Q-dependence of the full width at half-maximum (FWHM) of individual fcc(II) peaks ($x = 2.9$ sample). In addition to an overall monotonically increasing FWHM with increasing Q, all reflections with $h = k = l$ are markedly sharper (circled symbols), indicating the presence of stacking faults. The solid line is a guide to the eye.

REFERENCES AND NOTES

1. R. M. Fleming *et al.*, in *Clusters and Cluster-Assembled Materials, Materials Research Society Symposium*

Proceedings **206**, R. S. Averback, J. Bernholc, D. L. Nelson, Eds. (Materials Research Society, Pittsburgh, 1991), p. 691.
2. P. A. Heiney *et al.*, *Phys. Rev. Letters* **66**, 2911 (1991); J. E. Fischer *et al.*, *Science* **252**, 1288 (1991).
3. P. W. Stephens *et al.*, *Nature* **351**, 632 (1991).
4. R. M. Fleming *et al.*, *ibid.*, in press.
5. J. P. McCauley, Jr., *et al.*, *J. Am. Chem. Soc.*, in press.
6. K. Holczer *et al.*, *Synthetic Metals*, in press; P. W. Stephens *et al.*, in preparation.
7. R. M. Fleming *et al.*, *Nature* **352**, 701 (1991).
8. O. Zhou *et al.*, *ibid.* **351**, 462 (1991).
9. S. A. Safran, in *Solid State Physics*, H. Ehrenreich, F. Seitz, D. Turnbull, Eds. (Academic Press, New York, 1987), vol. 40, p. 183.
10. J. Ma, H.-Y. Choi, E. J. Mele, J. E. Fischer, *Synthetic Metals* **27**, A75 (1988).
11. D. M. Poirier *et al.*, *Science* **253**, 646 (1991).
12. C. T. Chen *et al.*, *Nature* **352**, 603 (1991).
13. J. E. Fischer, in *Chemical Physics of Intercalation*, A. P. Legrand and S. Flandrois, Eds. (Plenum, New York, 1987), p. 59.
14. R. C. Haddon *et al.*, *Nature* **350**, 320 (1991).
15. R. Tycko *et al.*, *Science* **253**, 884 (1991).
16. D. Djurado *et al.*, *Synthetic Metals* **34**, 683 (1989); P. A. Heiney *et al.*, *Phys. Rev.* **B42**, 2507 (1991).
17. S. C. Erwin and W. E. Pickett, *Science*, in press; private communication.
18. S. E. Millman and G. Kirczenow, *Phys. Rev.* **B26**, 2310 (1982).
19. D. E. Luzzi *et al.*, *J. Mat. Res.*, in press.
20. W. Andreoni, F. Gygi, M. Parrinello, in preparation.

21. We acknowledge helpful discussions with A. Cheng, P. A. Heiney, and E. J. Mele, and thank C. L. Lin for performing the magnetization measurements. This work was supported by the National Science Foundation Materials Research Laboratory Program, DMR88-19885, by NSF DMR89-01219, and by the Department of Energy, DE-FC02-86ER45254 and DE-FG05-90ER75596.

5 September 1991; accepted 20 September 1991

Clathrate Hydrate Formation in Amorphous Cometary Ice Analogs in Vacuo

DAVID BLAKE,* LOUIS ALLAMANDOLA, SCOTT SANDFORD,
DOUG HUDGINS, FRIEDEMANN FREUND

The presence of clathrate hydrates in cometary ice has been suggested to account for anomalous gas release at large radial distances from the sun as well as the retention of volatiles in comets to elevated temperatures. However, how clathrate hydrates can form in low-pressure environments, such as in cold interstellar molecular clouds, in the outer reaches of the early solar nebula, or in cometary ices, has been poorly understood. Experiments performed with the use of a modified electron microscope demonstrate that during the warming of vapor-deposited amorphous ices in vacuo, clathrate hydrates can form by rearrangements in the solid state. Phase separations and microporous textures that are the result of these rearrangements may account for a variety of anomalous cometary phenomena.

IN COLD INTERSTELLAR MOLECULAR clouds, gaseous species such as H_2O, CO, CO_2, CH_3OH, H_2CO, and NH_3 are believed to condense onto submicron silicate and carbonaceous grains to form icy mantles (*1, 2*). By a combination of processes that include gas-grain chemical reactions, ultraviolet photolysis, and cosmic-ray bombardment, these components can react further to produce small amounts of complex organic compounds (*3–7*). Icy planetesimals that probably formed through successive aggregation and agglomeration of such ice-coated grains may have carried significant amounts of prebiotic organic materials to Earth during its early history (*8*). Comets are thought to contain primitive and pristine materials from the early solar system, perhaps even unaltered interstellar grains (*1*). A knowledge of the properties of cometary ice (composition, structure state, and so forth) may therefore provide a better understanding of the types and amounts of volatiles and biogenic elements that were delivered to the early Earth.

During the past decade, several workers have probed the chemical composition and photochemical and photophysical properties of cometary and astrophysical ice analogs and compared the results with astronomical infrared data (*1, 9, 10*). In other work, the gas release properties of precometary and cometary ice analogs have been studied in order to understand the dynamics of comets and other icy solar system bodies (*11–13*). Although there have been some recent reports on structural investigations of mixed molecular ices (*14*), the crystallographic, microtextural, and phase evolution of astrophysical ice analogs specifically under high-vacuum conditions have not been investigated and are poorly understood. In order to make such observations, we modified an Hitachi H-500H Analytical Electron Microscope to enable us to study ices between 12 and 373 K (±2 K accuracy, measured at the sample) in a vacuum of 10^{-6} to 10^{-7} torr (*15*). Gas mixtures were bled into the vacuum and condensed onto cold (85 K), thin-film carbon substrates. The mixed molecular ices thus formed were characterized by transmission electron microscopy (TEM) and selected area electron diffraction (SAED). Through the use of a low electron dose imaging system, ice samples could be viewed without apparent structural damage or heating by the electron beam. We initially chose the system H_2O-CH_3OH because CH_3OH appears to be an important constituent in some cold interstellar clouds (*2, 10*) and has recently been detected in the comae of several comets (*16*).

We produced a compact, nonporous layer of amorphous ice 100 to 200 nm in thickness by condensing an H_2O:CH_3OH (2:1) gas mixture onto the 85 K substrate at a rate of 20 to 40 nm min^{-1}. Upon heating slowly at a rate of ~1 K min^{-1}, the ice remained amorphous until about 120 K, at which point broad Debye-Scherrer rings appeared in the SAED pattern. Bright-field TEM micrographs revealed the presence of two phases that were tightly intergrown on a scale length of about 0.1 μm (Fig. 1A). In the micrograph, amorphous areas appear bright and crystalline areas appear dark because diffracted electrons from the crystalline regions do not contribute to the final image. By 130 K the number of Debye-Scherrer rings had reached seven to eight (Fig. 1B). At about 145 K one of the two tightly intergrown phases sublimed, and a microporous texture was left (Fig. 1C) that produced an SAED pattern that could be indexed as the hexagonal polymorph of H_2O ice (Fig. 1D). We interpret the bright contrast features in Fig. 1C to be voids because in thin areas of the ice, the underlying carbon support film could be clearly seen within each of the features. At about 155 K the hexagonal H_2O ice rapidly sublimed.

Another sample of amorphous H_2O:CH_3OH (2:1) ice was warmed up more rapidly (~4 K min^{-1}) from 85 to 130 K. At 130 K the same SAED pattern was obtained as after slow warm-up, but the Debye-Scherrer rings were slightly sharper. In addition, a large number of single crystal spots could be seen. With the exception of a weak- to medium-intensity ring at ~3.6 Å [probably the (111) maximum of cubic H_2O ice], the powder rings and single-crystal spots could be indexed to a type II clathrate hydrate structure (space group *Fd3m*) (*17, 18*) with an *a*-parameter of 16.3 Å (Table 1) (*19*). In two earlier studies clathrate hydrates were inferred to have

---

D. Blake, Planetary Biology Branch, Mail Stop 239-4, National Aeronautics and Space Administration, Ames Research Center, Moffett Field, CA 94035.
L. Allamandola, S. Sandford, D. Hudgins, Mail Stop 245-6, Astrophysics Branch, National Aeronautics and Space Administration, Ames Research Center, Moffett Field, CA 94035.
F. Freund, Department of Physics, San Jose State University, San Jose, CA 95192.

*To whom correspondence should be addressed.